Unconventional quantum antiferromagnetism with a fourfold symmetry breaking in a spin-$\frac{1}{2}$ Ising-Heisenberg pentagonal chain

Katarína Karľová,[1,*] Jozef Strečka,[1] and Marcelo L. Lyra[2]

[1]*Institute of Physics, Faculty of Science, P. J. Šafárik University, Park Angelinum 9, 04001 Košice, Slovakia*
[2]*Instituto de Fisica, Universidade Federal de Alagoas, 57072-970 Maceió, AL, Brazil*

The spin-$\frac{1}{2}$ Ising-Heisenberg pentagonal chain is investigated with use of the star-triangle transformation, which establishes a rigorous mapping equivalence with the effective spin-$\frac{1}{2}$ Ising zigzag ladder. The investigated model has a rich ground-state phase diagram including two spectacular quantum antiferromagnetic ground states with a fourfold broken symmetry. It is demonstrated that these long-period quantum ground states arise due to a competition between the effective next-nearest-neighbor and nearest-neighbor interactions of the corresponding spin-$\frac{1}{2}$ Ising zigzag ladder. The concurrence is used to quantify the bipartite entanglement between the nearest-neighbor Heisenberg spin pairs, which are quantum-mechanically entangled in two quantum ground states with or without spontaneously broken symmetry. The pair correlation functions between the nearest-neighbor Heisenberg spins as well as the next-nearest-neighbor and nearest-neighbor Ising spins were investigated with the aim to bring insight into how a relevant short-range order manifests itself at low enough temperatures. It is shown that the specific heat displays temperature dependencies with either one or two separate round maxima.

I. INTRODUCTION

Crystalline magnetic materials with antiferromagnetic interactions are said to be geometrically frustrated if an elementary unit cell of the underlying magnetic lattice involves polygons with an odd number of spins [1–3]. The term "frustration" describes a situation in which, in the ground state of the corresponding classical spin system, not all pairwise spin-spin interactions can be satisfied simultaneously [4,5]. As a result, the geometrically frustrated magnetic materials exhibit at low enough temperatures a variety of fascinating phenomena [6]. The geometric spin frustration arising from the competition of antiferromagnetic interactions has been studied comprehensively within the framework of classical Ising spin systems, quantum Heisenberg spin systems, as well as semiclassical Ising-Heisenberg spin systems [7–9]. It is worthwhile to remark that the most common geometrically frustrated spin systems involve antiferromagnetically coupled spins situated on triangular cells. Among the most widely studied frustrated spin systems of this type, one could mention (i) one-dimensional lattices with the geometry of a diamond chain, a sawtooth chain, a zigzag ladder, an orthogonal-dimer chain; (ii) two-dimensional lattices such as a triangular lattice, a kagomé lattice, or a Shastry-Sutherland lattice; or (iii) three-dimensional lattices such as a pyrochlore lattice [7–9].

Contrary to this, much less attention has been paid so far to geometrically frustrated antiferromagnetic spin systems, which involve antiferromagnetically coupled spins situated on a pentagon as another frustrated polygon with an odd number of spins in an elementary unit cell. Such spins are present, for instance, in a discrete pentacopper cluster Cu_5 [10] or

a giant Keplerate molecule Fe_{30} with the shape of an icosidodecahedron [11,12]. The frustrated spin-$\frac{1}{2}$ Ising model on the Cairo pentagonal lattice was investigated in Refs. [13,14], while the magnetic properties of one-dimensional correlated electron systems with a pentagonal geometry were examined in Refs. [15–17]. The spin-$\frac{1}{2}$ Heisenberg antiferromagnet on the Cairo pentagonal lattice was investigated in Refs. [18–22] in relation to two iron-based experimental representatives—$Bi_2Fe_4O_9$ [23] and $Bi_4Fe_5O_{13}F$ [24]—of this outstanding magnetic structure. Recently, it was demonstrated that the spin-$\frac{1}{2}$ Ising-Heisenberg pentagonal chain of Cairo type exhibits many intriguing quantum ground states, including the frustrated ones with a nonzero residual entropy (i.e., high macroscopic degeneracy) [25].

In this work, we will investigate another version of the spin-$\frac{1}{2}$ Ising-Heisenberg pentagonal chain, whose magnetic structure is motivated by the polymeric coordination compound $[\{CuL\}Gd(H_2O)_3\{Fe(CN)_6\}]\cdot 4H_2O$, to be further abbreviated as CuGdFe [26]. The magnetic structure of the CuGdFe compound consists of low-spin Fe^{3+} ions ($S = 1/2$) with a relatively high magnetic anisotropy and the almost isotropic Cu^{2+} ($S = 1/2$) and Gd^{3+} ($S = 7/2$) ions. For the sake of simplicity, the magnetically anisotropic Fe^{3+} ions will be approximated by the notion of classical Ising spins, while the magnetically isotropic Cu^{2+} and Gd^{3+} ions will be treated as quantum Heisenberg spins all of size $\frac{1}{2}$. In contrast to our expectations, the present version of the spin-$\frac{1}{2}$ Ising-Heisenberg pentagonal chain does not display any highly degenerate ground state because, surprisingly, a competition between exchange couplings stabilizes a long-period quantum antiferromagnetic ground state instead.

The organization of this paper is as follows. The spin-$\frac{1}{2}$ Ising-Heisenberg pentagonal chain will be defined in Sec. II, where a few details of the calculation procedure will also be
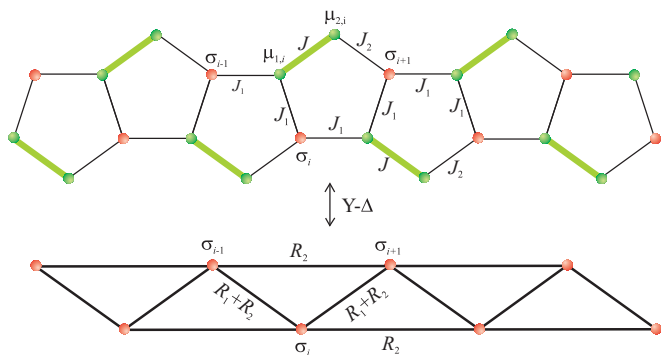
---

*katarina.karlova@student.upjs.sk

FIG. 1. A schematic representation of the spin-$\frac{1}{2}$ Ising-Heisenberg pentagonal chain (upper panel) and the effective spin-$\frac{1}{2}$ Ising zigzag ladder (lower panel) obtained after applying the star-triangle mapping transformation.

presented. The most interesting results for the ground-state phase diagram, pair correlation functions, concurrence, and specific heat will be discussed in Sec. III. Finally, we will end our study with several concluding remarks mentioned in Sec. IV.

II. ISING-HEISENBERG PENTAGONAL CHAIN

Let us consider the spin-$\frac{1}{2}$ Ising-Heisenberg pentagonal chain, which is composed of edge-sharing pentagons as depicted in the upper panel of Fig. 1. Note that each elementary pentagon involves one couple of Heisenberg spins ($\mu_{1,i}, \mu_{2,i}$) and three enclosing Ising spins (σ_{i-1}, σ_i, and σ_{i+1}). The spin-$\frac{1}{2}$ Ising-Heisenberg pentagonal chain can then be defined through the following Hamiltonian:

$$\hat{\mathcal{H}} = J \sum_{i=1}^{N} \left[\Delta \left(\hat{\mu}_{1,i}^x \hat{\mu}_{2,i}^x + \hat{\mu}_{1,i}^y \hat{\mu}_{2,i}^y \right) + \hat{\mu}_{1,i}^z \hat{\mu}_{2,i}^z \right]$$
$$+ J_1 \sum_{i=1}^{N} \hat{\mu}_{1,i}^z \left(\hat{\sigma}_{i-1}^z + \hat{\sigma}_i^z \right) + J_2 \sum_{i=1}^{N} \hat{\mu}_{2,i}^z \hat{\sigma}_{i+1}^z. \quad (1)$$

Here, $\hat{\mu}_{j,i}^\alpha$ ($j = 1,2$; $\alpha = x,y,z$) and $\hat{\sigma}_i^z$ denote spatial components of the spin-$\frac{1}{2}$ operators, the parameter $J > 0$ labels the antiferromagnetic nearest-neighbor interaction between the Heisenberg spins, the coupling constants J_1 and J_2 determine two nearest-neighbor interactions between the Ising and Heisenberg spins, and N denotes the total number of pentagonal unit cells. Finally, the parameter Δ determines an exchange anisotropy in the XXZ Heisenberg interaction. For the sake of simplicity, the periodic boundary conditions are imposed under the constraints $\sigma_i \equiv \sigma_{N+i}$.

The total Hamiltonian (1) can be alternatively rewritten as a sum over cluster Hamiltonians

$$\hat{\mathcal{H}} = \sum_{i=1}^{N} \hat{\mathcal{H}}_i, \quad (2)$$

where the ith cluster Hamiltonian $\hat{\mathcal{H}}_i$ contains all the interaction terms involving the ith Heisenberg dimer

$$\hat{\mathcal{H}}_i = J \left[\Delta \left(\hat{\mu}_{1,i}^x \hat{\mu}_{2,i}^x + \hat{\mu}_{1,i}^y \hat{\mu}_{2,i}^y \right) + \hat{\mu}_{1,i}^z \hat{\mu}_{2,i}^z \right]$$
$$+ J_1 \hat{\mu}_{1,i}^z \left(\hat{\sigma}_{i-1}^z + \hat{\sigma}_i^z \right) + J_2 \hat{\mu}_{2,i}^z \hat{\sigma}_{i+1}^z. \quad (3)$$

The cluster Hamiltonians obviously commute with each other, $[\hat{\mathcal{H}}_j, \hat{\mathcal{H}}_k] = 0$, and thus the partition function of the spin-$\frac{1}{2}$ Ising-Heisenberg pentagonal chain can be written in the factorized form

$$\mathcal{Z} = \sum_{\{\sigma\}} \mathrm{Tr} \exp(-\beta \hat{\mathcal{H}}) = \sum_{\{\sigma\}} \prod_{i=1}^{N} \mathrm{Tr}_{[\mu_{1,i}, \mu_{2,i}]} \exp(-\beta \hat{\mathcal{H}}_i)$$
$$= \sum_{\{\sigma\}} \prod_{i=1}^{N} \mathcal{Z}_i, \quad (4)$$

where $\beta = 1/(k_B T)$, k_B is Boltzmann's constant, T is the absolute temperature, and the symbol $\sum_{\{\sigma\}}$ marks a summation over all possible spin configurations of the Ising spins. In the above, we have introduced notation for the expression

$$\mathcal{Z}_i = \mathrm{Tr}_{[\mu_{1,i}, \mu_{2,i}]} \exp(-\beta \hat{\mathcal{H}}_i), \quad (5)$$

which represents the effective Boltzmann's factor obtained after tracing out spin degrees of freedom of the ith couple of the Heisenberg spins. To proceed further, one necessarily needs to evaluate the effective Boltzmann's factor $\mathcal{Z}_i$ given by Eq. (5). For this purpose, it is quite advisable to use a matrix representation of the cluster Hamiltonian $\hat{\mathcal{H}}_i$ in the basis spanned over four available states of two Heisenberg spins $\mu_{1,i}$ and $\mu_{2,i}$,

$$|\uparrow, \uparrow\rangle_i = |\uparrow\rangle_{1,i} |\uparrow\rangle_{2,i}, \quad |\uparrow, \downarrow\rangle_i = |\uparrow\rangle_{1,i} |\downarrow\rangle_{2,i},$$
$$|\downarrow, \uparrow\rangle_i = |\downarrow\rangle_{1,i} |\uparrow\rangle_{2,i}, \quad |\downarrow, \downarrow\rangle_i = |\downarrow\rangle_{1,i} |\downarrow\rangle_{2,i}. \quad (6)$$

The state vectors $|\uparrow\rangle_{k,i}$ and $|\downarrow\rangle_{k,i}$ ($k = 1,2$) denote two eigenvectors of the spin operator $\hat{\mu}_{k,i}^z$ with the respective eigenvalues $\mu_{k,i}^z = \pm 1/2$. After a straightforward diagonalization of the cluster Hamiltonian $\hat{\mathcal{H}}_i$, one obtains the following four eigenvalues:

$$E_{i1,i2} = \frac{J}{4} \pm \left[\frac{J_1}{2} \left(\sigma_{i-1}^z + \sigma_i^z \right) + \frac{J_2}{2} \sigma_{i+1}^z \right],$$
$$E_{i3,i4} = -\frac{J}{4} \pm \frac{1}{2} \sqrt{ \left[J_1 \left(\sigma_{i-1}^z + \sigma_i^z \right) - J_2 \sigma_{i+1}^z \right]^2 + (J\Delta)^2 }$$
$$(7)$$

and the corresponding eigenvectors

$$|\varphi_{1,i}\rangle = |\uparrow\rangle_{1,i} |\uparrow\rangle_{2,i},$$
$$|\varphi_{2,i}\rangle = |\downarrow\rangle_{1,i} |\downarrow\rangle_{2,i},$$
$$|\varphi_{3,i}\rangle = c_1 |\uparrow\rangle_{1,i} |\downarrow\rangle_{2,i} + c_2 |\downarrow\rangle_{1,i} |\uparrow\rangle_{2,i},$$
$$|\varphi_{4,i}\rangle = c_2 |\uparrow\rangle_{1,i} |\downarrow\rangle_{2,i} - c_1 |\downarrow\rangle_{1,i} |\uparrow\rangle_{2,i}, \quad (8)$$

where

$$c_1 = \frac{1}{\sqrt{2}} \left[1 + \frac{J_1 \left(\sigma_{i-1}^z + \sigma_i^z \right) - J_2 \sigma_{i+1}^z}{\sqrt{ \left[J_1 \left(\sigma_{i-1}^z + \sigma_i^z \right) - J_2 \sigma_{i+1}^z \right]^2 + (J\Delta)^2 }} \right]^{\frac{1}{2}},$$

$$c_2 = \frac{1}{\sqrt{2}} \left[1 - \frac{J_1 \left(\sigma_{i-1}^z + \sigma_i^z \right) - J_2 \sigma_{i+1}^z}{\sqrt{ \left[J_1 \left(\sigma_{i-1}^z + \sigma_i^z \right) - J_2 \sigma_{i+1}^z \right]^2 + (J\Delta)^2 }} \right]^{\frac{1}{2}}.$$
$$(9)$$

Now, one may use the eigenvalues (7) for a simple calculation of the Boltzmann's factor (5). The resulting expression immediately implies the possibility of performing the generalized star-triangle transformation [27–30]

$$
\mathcal{Z}_i = \mathrm{Tr}_{[\mu_{i,1},\mu_{i,2}]} \exp(-\beta \hat{\mathcal{H}}_i) = \sum_{j=1}^{4} \exp(-\beta E_{ij})
$$

$$
= 2 \exp\left(-\frac{\beta J}{4}\right) \cosh\left\{\frac{\beta}{2}\left[J_1(\sigma_{i-1}^z + \sigma_i^z) + J_2\sigma_{i+1}\right]\right\} + 2\exp\left(\frac{\beta J}{4}\right)\cosh\left\{\frac{\beta}{2}\sqrt{\left[J_1(\sigma_{i-1}^z + \sigma_i^z) - J_2\sigma_{i+1}^z\right]^2 + (J\Delta)^2}\right\}
$$

$$
= A\exp[\beta(R_1\sigma_{i-1}\sigma_i + R_2\sigma_i\sigma_{i+1} + R_2\sigma_{i-1}\sigma_{i+1})]. \tag{10}
$$

From the physical point of view, the mapping transformation (10) effectively removes all the interaction parameters associated with the ith couple of the Heisenberg spins from the pentagonal unit cell and replaces them by the effective interactions R_1 and R_2 between the three enclosing Ising spins σ_{i-1}, σ_i, and σ_{i+1} (see Fig. 2). In this way, one establishes a simple mapping correspondence between the spin-$\frac{1}{2}$ Ising-Heisenberg pentagonal chain and the spin-$\frac{1}{2}$ Ising zigzag ladder with the effective nearest-neighbor and next-nearest-neighbor interactions $R_1 + R_2$ and R_2, respectively (see the lower panel of Fig. 1). Moreover, the mapping transformation (10) must hold for all possible spin combinations of the Ising spins σ_{i-1}, σ_i, and σ_{i+1}. This "self-consistency" condition then unambiguously determines the as yet unspecified mapping parameters A, R_1, and R_2,

$$
A = \left(V_1 V_2 V_3^2\right)^{1/4}, \quad \beta R_1 = \ln\left(\frac{V_1 V_2}{V_3^2}\right), \quad \beta R_2 = \ln\left(\frac{V_1}{V_2}\right), \tag{11}
$$

which are given by the functions V_1, V_2, and V_3 defined as

$$
V_1 = \mathcal{Z}_i\left(\pm\frac{1}{2},\pm\frac{1}{2},\pm\frac{1}{2}\right) = 2\exp\left(-\frac{\beta J}{4}\right)\cosh\left(\frac{\beta J_1}{2} + \frac{\beta J_2}{4}\right) + 2\exp\left(\frac{\beta J}{4}\right)\cosh\left[\frac{\beta}{4}\sqrt{(2J_1 - J_2)^2 + (2J\Delta)^2}\right],
$$

$$
V_2 = \mathcal{Z}_i\left(\mp\frac{1}{2},\mp\frac{1}{2},\pm\frac{1}{2}\right) = 2\exp\left(-\frac{\beta J}{4}\right)\cosh\left(\frac{\beta J_1}{2} - \frac{\beta J_2}{4}\right) + 2\exp\left(\frac{\beta J}{4}\right)\cosh\left[\frac{\beta}{4}\sqrt{(2J_1 + J_2)^2 + (2J\Delta)^2}\right],
$$

$$
V_3 = \mathcal{Z}_i\left(\pm\frac{1}{2},\mp\frac{1}{2},\mp\frac{1}{2}\right) = \mathcal{Z}_i\left(\mp\frac{1}{2},\pm\frac{1}{2},\mp\frac{1}{2}\right) = 2\exp\left(-\frac{\beta J}{4}\right)\cosh\left(\frac{\beta J_2}{4}\right) + 2\exp\left(\frac{\beta J}{4}\right)\cosh\left[\frac{\beta}{4}\sqrt{J_2^2 + (2J\Delta)^2}\right]. \tag{12}
$$

The partition function of the spin-$\frac{1}{2}$ Ising-Heisenberg pentagonal chain can be subsequently calculated from the mapping correspondence with the partition function of the spin-$\frac{1}{2}$ Ising zigzag ladder,

$$
\mathcal{Z}(\beta, J, J_1, J_2) = A^N \mathcal{Z}_{z-z}(\beta, K_1 = R_1 + R_2, K_2 = R_2). \tag{13}
$$

The effective interactions of the corresponding spin-$\frac{1}{2}$ Ising zigzag ladder are given by Eqs. (11) and (12), and the effective model can be defined through the following Hamiltonian:

$$
\mathcal{H}_{z-z} = -K_1 \sum_{i=1}^{N} \sigma_{i-1}^z \sigma_i^z - K_2 \sum_{i=1}^{N} \sigma_{i-1}^z \sigma_{i+1}^z. \tag{14}
$$

It should be stressed that the effective temperature-dependent nearest-neighbor interaction $K_1 = R_1 + R_2$ differs from the
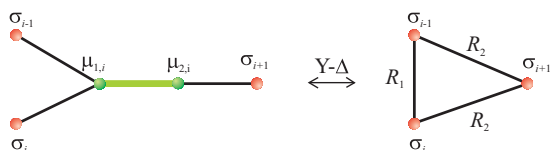

FIG. 2. A diagrammatic representation of the star-triangle mapping transformation, which allows us to replace degrees of freedom of the ith Heisenberg spin pair through the effective interactions between the three enclosing Ising spins.

effective temperature-dependent next-nearest-neighbor interaction $K_2 = R_2$ due to the presence of the additional interaction term R_1. The partition function of the spin-$\frac{1}{2}$ Ising zigzag ladder can be rigorously calculated within the framework of the standard transfer-matrix approach [31–36],

$$
\mathcal{Z}_{z-z} = \sum_{\{\sigma\}} \prod_{i=1}^{N} \langle\sigma_{i-1},\sigma_i|T|\sigma_i,\sigma_{i+1}\rangle, \tag{15}
$$

where the expression $\langle\sigma_{i-1},\sigma_i|T|\sigma_i,\sigma_{i+1}\rangle$ denotes the transfer matrix defined by

$$
\langle\sigma_{i-1},\sigma_i|T|\sigma_i,\sigma_{i+1}\rangle
$$
$$
= \exp\left[\frac{\beta K_1}{2}(\sigma_{i-1}\sigma_i + \sigma_i\sigma_{i+1}) + \beta K_2\sigma_{i-1}\sigma_{i+1}\right]. \tag{16}
$$

Recall that the periodic boundary conditions $\sigma_N \equiv \sigma_0$ and $\sigma_{N+1} \equiv \sigma_1$ are assumed. The partition function of the spin-$\frac{1}{2}$ Ising zigzag ladder is given through four transfer-matrix eigenvalues

$$
\mathcal{Z}_{z-z} = \mathrm{Tr}\,T^N = \mathrm{Tr}\,\Lambda^N = \lambda_1^N + \lambda_2^N + \lambda_3^N + \lambda_4^N, \tag{17}
$$

which have the following explicit form:

$$
\lambda_1 = \exp\left(\frac{\beta K_2}{4}\right)\left[\cosh\left(\frac{\beta K_1}{4}\right) + \sqrt{\sinh^2\left(\frac{\beta K_1}{4}\right) + \exp\left(-\beta K_2\right)}\right],
$$

$$
\lambda_2 = \exp\left(\frac{\beta K_2}{4}\right)\left[\cosh\left(\frac{\beta K_1}{4}\right) - \sqrt{\sinh^2\left(\frac{\beta K_1}{4}\right) + \exp\left(-\beta K_2\right)}\right], \tag{18}
$$

$$
\lambda_{3,4} = \exp\left(\frac{\beta K_2}{4}\right)\left[\sinh\left(\frac{\beta K_1}{4}\right) \pm \sqrt{\cosh^2\left(\frac{\beta K_1}{4}\right) - \exp\left(-\beta K_2\right)}\right].
$$

All thermodynamic functions are given in the thermodynamic limit $N \to \infty$ only through the largest transfer-matrix eigenvalue $\mathcal{Z}_{z-z} = \lambda_1^N$. According to Eq. (13), the exact closed-form expression for the partition function of the spin-$\frac{1}{2}$ Ising-Heisenberg pentagonal chain then reads

$$
\mathcal{Z} = (A\lambda_1)^N. \tag{19}
$$

Next, one may also calculate all thermodynamic quantities of interest for the spin-$\frac{1}{2}$ Ising-Heisenberg pentagonal chain. For, instance, the Helmholtz free energy per unit cell is given by

$$
f = -k_{\mathrm{B}}T \ln A - k_{\mathrm{B}}T \ln \lambda_1. \tag{20}
$$

The entropy and the specific heat per unit cell can then be calculated according to the formulas

$$
s = -\frac{\partial f}{\partial T}, \quad c = -T\frac{\partial^2 f}{\partial T^2}. \tag{21}
$$

To bring insight into a local spin arrangement emerging within ground states of the spin-$\frac{1}{2}$ Ising-Heisenberg pentagonal chain, one may easily calculate also several local spin-spin correlation functions according to the formulas

$$
C_{hh}^{zz} = \left\langle \hat{\mu}_{i,1}^z \hat{\mu}_{i,2}^z \right\rangle = -\frac{1}{N}\frac{\partial \ln \mathcal{Z}}{\partial \beta J},
$$

$$
C_{hh}^{xx} = \left\langle \hat{\mu}_{i,1}^x \hat{\mu}_{i,2}^x \right\rangle = -\frac{1}{N}\frac{\partial \ln \mathcal{Z}}{\partial \beta J \Delta},
$$

$$
C_{ii}^{nn} = \left\langle \hat{\sigma}_{i-1}^z \hat{\sigma}_i^z \right\rangle = \frac{1}{N}\frac{\partial \ln \mathcal{Z}_{z-z}}{\partial \beta K_1},
$$

$$
C_{ii}^{nnn} = \left\langle \hat{\sigma}_{i-1}^z \hat{\sigma}_{i+1}^z \right\rangle = \frac{1}{N}\frac{\partial \ln \mathcal{Z}_{z-z}}{\partial \beta K_2}. \tag{22}
$$

Note that the final explicit formulas for the correlation functions (22) are too cumbersome to write down here explicitly, but they can be obtained after performing the relevant differentiation. Two spatial components of the pair correlation function between the nearest-neighbor Heisenberg spins can be utilized for the calculation of the concurrence,

$$
C = 4\left|C_{hh}^{xx}\right| - \left|\frac{1}{2} + 2C_{hh}^{zz}\right|, \tag{23}
$$

which serves as a measure of bipartite entanglement [37–39].

III. RESULTS AND DISCUSSION

Let us start our discussion with a ground-state analysis of the spin-$\frac{1}{2}$ Ising-Heisenberg pentagonal chain with the anti-

ferromagnetic interaction $J > 0$ between the nearest-neighbor Heisenberg spins, which will henceforth serve as the energy unit. First, we will perform a closer inspection of the zero-temperature asymptotic behavior of various pair correlation functions. The correlation function between the z components of the nearest-neighbor Heisenberg spins C_{hh}^{zz} is depicted in the form of a density plot in Fig. 3(a) within the J_1/J-J_2/J plane. The correlation function C_{hh}^{zz} splits the parameter space into two different regions visible as dark gray (red) and light gray (yellow), which imply ferromagnetic and antiferromagnetic short-range ordering between the z components of the Heisenberg spins, respectively. Furthermore, the correlation function between the x components of the Heisenberg spins shown in Fig. 3(b) suggests that off-diagonal correlations are totally absent in the dark gray (red) region, while they imply antiferromagnetic short-range correlations between x and y components of the nearest-neighbor Heisenberg spins in the rest of the parameter space.

A density plot for the correlation function between the nearest-neighbor Ising spins C_{ii}^{nn} is presented in Fig. 3(c). According to this plot, one detects the parameter region (dark gray or red) with perfect ferromagnetic short-range order beside the parameter region (light gray or orange) with a complete absence of short-range correlation between the nearest-neighbor Ising spins. A zero value of the correlation function C_{ii}^{nn} could be consistent either with a complete randomness of the Ising spins or an equal contribution of ferromagnetic and antiferromagnetic nearest-neighbor correlations. However, the first option is excluded by the correlation function between the next-nearest-neighbor Ising spins C_{ii}^{nnn} depicted in Fig. 3(d), since it gains the strongest possible antiferromagnetic correlation $C_{ii}^{nnn} = -1/4$ in this parameter region (light gray or yellow). In the rest of the parameter space, one finds ferromagnetic short-range correlations between the Ising spins, in agreement with the extremal values of the nearest-neighbor and next-nearest-neighbor correlation functions $C_{ii}^{nn} = 1/4$ and $C_{ii}^{nnn} = 1/4$ [dark gray or red in Figs. 3(c) and 3(d)].

An independent confirmation of the aforementioned results can be obtained from a comprehensive analysis of the lowest-energy eigenstates of the spin-$\frac{1}{2}$ Ising-Heisenberg pentagonal chain, which allows us to construct the ground-state phase diagram displayed in Fig. 3(e) in the J_1/J-J_2/J plane. As one can see, the ground-state phase diagram involves three phases I, II, and III along with their three mirror images I′, II′, and III′ with flipped Ising spins, which are connected through an inversion symmetry center located at the axes origin
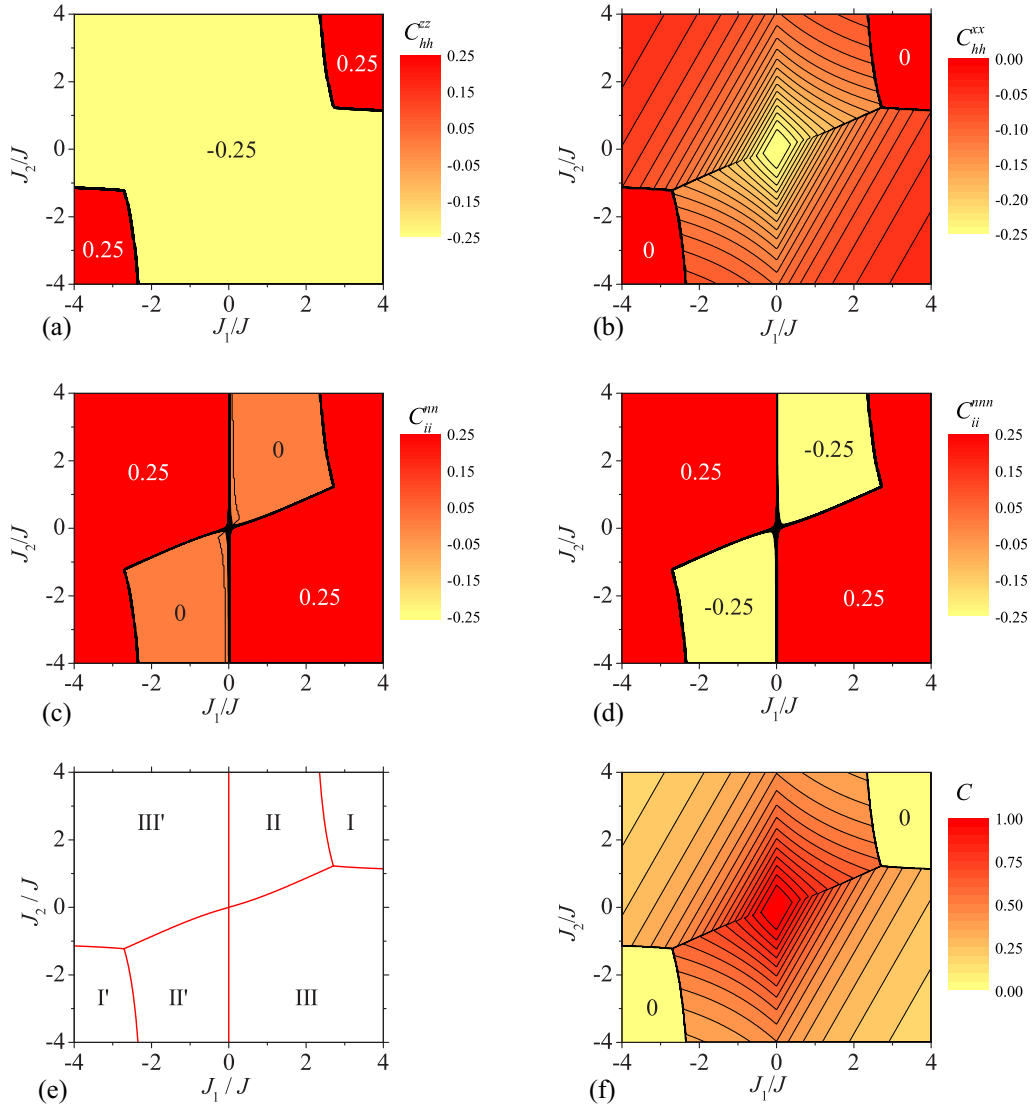
FIG. 3. Zero-temperature density plots for (a) the correlation function between the z components of the Heisenberg spins; (b) the correlation function between the x components of the Heisenberg spins; (c) the correlation function between the nearest-neighbor Ising spins; (d) the correlation function between the next-nearest-neighbor Ising spins; (e) the ground-state phase diagram in the J_1/J-J_2/J plane; and (f) zero-temperature density plot for the concurrence of the Heisenberg spin pairs. The quoted numbers determine specific values of the relevant quantities in a given parameter space.

$[J_1, J_2] = [0,0],$

$$|\text{I}\rangle = \prod_{i=1}^{N} |\downarrow\rangle_{\sigma_i} |\varphi_{1,i}\rangle, \quad |\text{I}'\rangle = \prod_{i=1}^{N} |\uparrow\rangle_{\sigma_i} |\varphi_{1,i}\rangle,$$

$$|\text{II}\rangle = \prod_{i=1}^{N/4} |\uparrow\rangle_{\sigma_{4i-3}} |\uparrow\rangle_{\sigma_{4i-2}} |\downarrow\rangle_{\sigma_{4i-1}} |\downarrow\rangle_{\sigma_{4i}} |\varphi_{4,4i-3}(|\uparrow\rangle_{\sigma_{4i-3}} |\uparrow\rangle_{\sigma_{4i-2}} |\downarrow\rangle_{\sigma_{4i-1}})\rangle |\varphi_{4,4i-2}(|\uparrow\rangle_{\sigma_{4i-2}} |\downarrow\rangle_{\sigma_{4i-1}} |\downarrow\rangle_{\sigma_{4i}})\rangle$$
$$\times |\varphi_{4,4i-1}(|\downarrow\rangle_{\sigma_{4i-1}} |\downarrow\rangle_{\sigma_{4i}} |\uparrow\rangle_{\sigma_{4i+1}})\rangle |\varphi_{4,4i}(|\downarrow\rangle_{\sigma_{4i}} |\uparrow\rangle_{\sigma_{4i+1}} |\uparrow\rangle_{\sigma_{4i+2}})\rangle,$$

$$|\text{II}'\rangle = \prod_{i=1}^{N/4} |\downarrow\rangle_{\sigma_{4i-3}} |\downarrow\rangle_{\sigma_{4i-2}} |\uparrow\rangle_{\sigma_{4i-1}} |\uparrow\rangle_{\sigma_{4i}} |\varphi_{4,4i-3}(|\downarrow\rangle_{\sigma_{4i-3}} |\downarrow\rangle_{\sigma_{4i-2}} |\uparrow\rangle_{\sigma_{4i-1}})\rangle |\varphi_{4,4i-2}(|\downarrow\rangle_{\sigma_{4i-2}} |\uparrow\rangle_{\sigma_{4i-1}} |\uparrow\rangle_{\sigma_{4i}})\rangle$$
$$\times |\varphi_{4,4i-1}(|\uparrow\rangle_{\sigma_{4i-1}} |\uparrow\rangle_{\sigma_{4i}} |\downarrow\rangle_{\sigma_{4i+1}})\rangle |\varphi_{4,4i}(|\uparrow\rangle_{\sigma_{4i}} |\downarrow\rangle_{\sigma_{4i+1}} |\downarrow\rangle_{\sigma_{4i+2}})\rangle,$$

$$|\text{III}\rangle = \prod_{i=1}^{N} |\uparrow\rangle_{\sigma_i} |\varphi_{4,i}(|\uparrow\rangle_{\sigma_{i-1}} |\uparrow\rangle_{\sigma_i} |\uparrow\rangle_{\sigma_{i+1}})\rangle, \quad |\text{III}'\rangle = \prod_{i=1}^{N} |\downarrow\rangle_{\sigma_i} |\varphi_{4,i}(|\downarrow\rangle_{\sigma_{i-1}} |\downarrow\rangle_{\sigma_i} |\downarrow\rangle_{\sigma_{i+1}})\rangle. \tag{24}$$
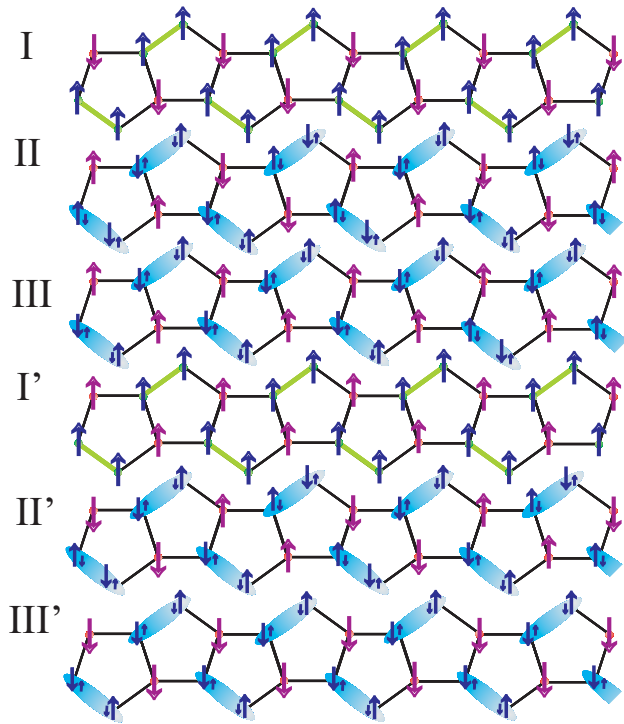
FIG. 4. A schematic representation of the ground states of the spin-$\frac{1}{2}$ Ising-Heisenberg pentagonal chain. Ellipses denote a singlet-like state, whereas greater (smaller) arrows denote the spin state with a higher (lower) occurrence probability.

In the above, the eigenvectors $|\varphi_{j,i}\rangle$ ($j = 1,4$) specifying eigenstates of the Heisenberg spin pairs are given by Eq. (8) and the states of three enclosing Ising spins quoted in parentheses determine through Eq. (9) the respective probability amplitudes entering into the eigenvector $|\varphi_{4,i}\rangle$. For illustrative purposes, all available ground states are visualized in Fig. 4. It is worthwhile to remark that each ground state is at least twofold-degenerate, because flipping all spins in the eigenvectors (24) provides, due to the validity of time-reversal symmetry at zero field, another eigenvector with the same energy. In addition, another eigenvector with the same energy can be obtained from the eigenvectors $|II\rangle$ and $|II'\rangle$ by a trivial shift of indices $i \rightarrow i + 1$ because of a peculiar fourfold symmetry breaking. Consequently, phases I, I′, III, and III′ are just twofold-degenerate, while phases II and II′ are fourfold degenerate. Phase I can be viewed as a classical ferrimagnetic state, phase I′ as a classical ferromagnetic state, phases II and II′ as modulated quantum antiferromagnetic states, phase III as a quantum ferrimagnetic state, and phase III′ as a quantum ferromagnetic state. The quantum character of the ground states II, II′, III, and III′ is verified by the concurrence depicted in Fig. 3(f), which exhibits nonzero values within these ground states in contrast with the classical ground states I and I′ with no concurrence.

The striking character of the long-period ground states II and II′ with fourfold symmetry breaking can be understood with the help of the effective spin-$\frac{1}{2}$ Ising zigzag ladder, for which a remarkable up-up-down-down spin configuration has the lowest energy upon assuming that the interaction ratio between next-nearest neighbors and nearest neighbors satisfies

the condition [32]

$$\frac{K_2}{|K_1|} = \frac{R_2}{|R_1 + R_2|} < -\frac{1}{2}. \tag{25}$$

Due to this fact, the spin-$\frac{1}{2}$ Ising-Heisenberg pentagonal chain exhibits a similar four-fold symmetry breaking within the ground states II and II′ whenever it falls into the parameter space specified by the condition (25). To verify this statement, let us investigate an asymptotic behavior of the effective couplings at low enough temperature as a function of the interaction ratio J_1/J and J_2/J depicted in Fig. 5. The highly nonmonotonic dependencies of the effective couplings R_1 and R_2 generally cause nontrivial dependencies of the effective nearest-neighbor interaction $|R_1 + R_2|$, which enters into the denominator of the condition (25). If the effective nearest-neighbor interaction turns to zero, i.e., $|R_1 + R_2| = 0$, then the relative ratio between the effective next-nearest-neighbor and nearest-neighbor interactions shows a striking divergence clearly seen in Figs. 5(a) and 5(b). Figure 5(a) depicts the effective couplings as a function of the interaction ratio J_1/J at the constant value of the other interaction parameter $J_2/J = 0.5$. Under this condition, the long-period phase II becomes the ground state within the interval $J_1/J \in (0; 1.26)$ in agreement with the ground-state phase diagram depicted in Fig. 3(e) and the condition (25). Figure 5(b) serves as evidence that the long-period ground state II becomes more stable at the constant value of the interaction parameter $J_2/J = 2$ because the condition (25) is satisfied over the wider interval of $J_1/J \in (0; 2.55)$. The effective interactions as a function of the interaction parameter J_2/J are depicted in Figs. 5(c) and 5(d) at the fixed value of the interaction ratio $J_1/J = 2$ and $J_1/J = 4$, respectively. In the former case, $J_1/J = 2$, the long-period phase II is maintained as the ground state for $J_2/J > 0.86$ when the condition (25) is still met [see Fig. 5(c)]. On the other hand, the relative ratio between the effective next-nearest-neighbor and nearest-neighbor couplings shown as a dotted-dashed (orange) line never crosses a dotted line in Fig. 5(d), which means that the condition (25) is never satisfied in the latter case, $J_1/J = 4$, in accordance with the absence of the long-period phase II in this parameter space.

Next, let us comment on the influence of temperature on two spatial components of the correlation function between the nearest-neighbor Heisenberg spins. The temperature dependence of the z component of the correlation function is shown in Fig. 6(a) for several values of the interaction ratio J_1/J by keeping the other interaction ratio $J_2/J = 0.5$ constant. The selected parameters either fall deep inside phases II and III or close to their phase boundary [see Fig. 3(e)]. It is noteworthy that zero-temperature asymptotic values of C_{hh}^{zz} corroborate the antiferromagnetic character of this correlation within both ground states II and III, in agreement with the previous ground-state analysis. The correlation function C_{hh}^{zz} generally diminishes with increasing temperature, whereas very low temperature is needed to override 80% of the correlations for the particular value $J_1/J = 2.5$ driving the investigated model in the vicinity of the triple coexistence point between the ground states I, II, and III. On the other hand, the increase of temperature can temporarily reinforce short-range correlations in a relatively wide region of moderate temperatures, as evidenced by a nonmonotonic dependence
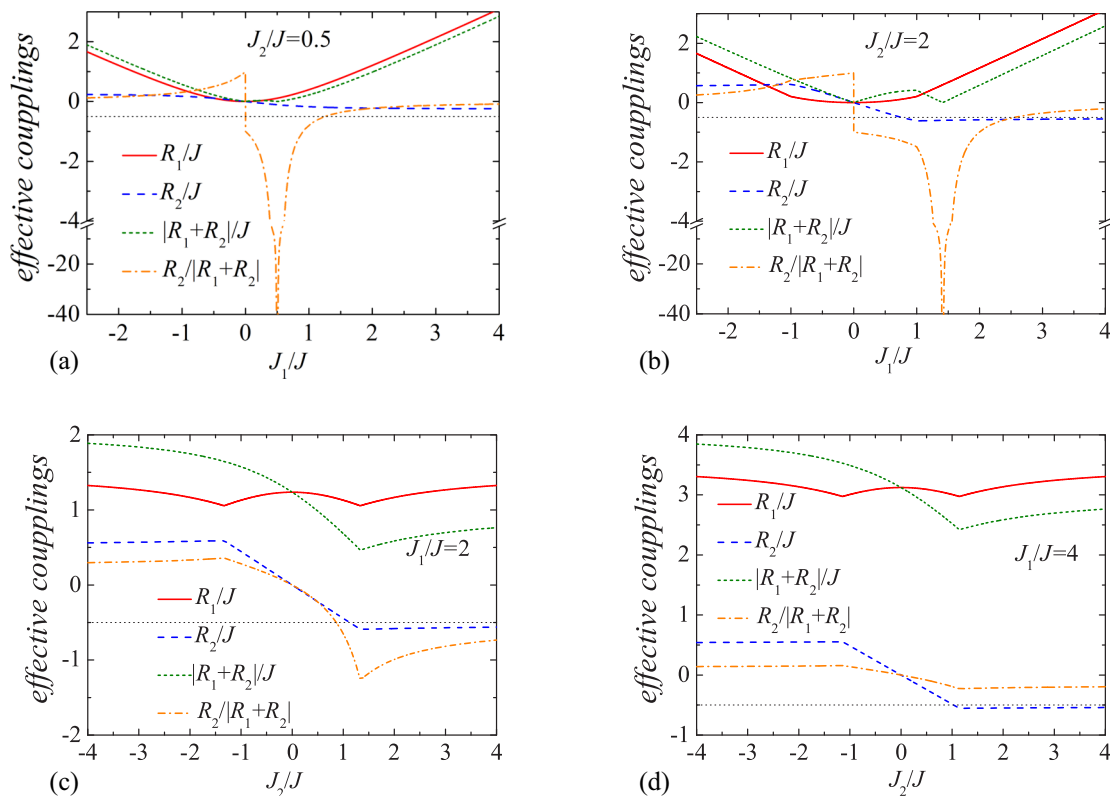
FIG. 5. The effective couplings of the equivalent spin-$\frac{1}{2}$ Ising zigzag ladder as a function of the interaction ratio at sufficiently low temperature $k_B T/J = 0.001$. The ground state of the effective spin-$\frac{1}{2}$ Ising zigzag ladder is driven by the relative strength of the next-nearest-neighbor interaction R_2 to the nearest-neighbor interaction $R_1 + R_2$, i.e., the ratio $R_2/|R_1 + R_2|$ plotted by a dashed-dotted line [see Eq. (25)]. The long-period quantum ground state II emerges if the relative ratio between both effective couplings is below the critical value $R_2/|R_1 + R_2| = -1/2$ plotted by a thin dotted line.

shown in Fig. 6(b) for the x component of the correlation function C_{hh}^{xx} for $J_1/J = 0.3$ and $J_2/J = 0.5$.

The z and x components of the correlation function between the nearest-neighbor Heisenberg spins are depicted in Figs. 6(c) and 6(d) when the interaction ratio $J_2/J = 2$ is fixed and the interaction parameter J_1/J either drives the investigated model deep inside phases I and II or close to their phase boundary. In agreement with our expectations, the correlation functions are less resistant against thermal fluctuations in the vicinity of the relevant phase boundary than deep inside of the individual ground states. Moreover, it is quite evident from Fig. 6(c) that the rising temperature may even invoke a striking ferromagnetic-to-antiferromagnetic crossover signaled by the vanishing of the correlation function C_{hh}^{zz}, which indicates the uncorrelated nature of the z component of the Heisenberg spin pairs at a certain "frustration" temperature [40].

The temperature dependencies of the z and x components of the correlation function between the nearest-neighbor Heisenberg spins are depicted in Figs. 7(a) and 7(b) for the constant value of the interaction parameter $J_1/J = 2$ and a few selected values of the parameter J_2/J falling either deep inside phases II and III or close to their phase boundaries [cf. Fig. 3(e)]. The appropriate zero-temperature limits are in concordance with Figs. 3(a) and 3(b), while the increasing temperature generally causes a gradual cancellation of the relevant short-range order. It can be understood from Fig. 7(a) that the z component of the correlation function C_{hh}^{zz} is less resistant against rising

temperature in phase II with a fourfold broken symmetry than in phase III without symmetry breaking. Contrary to this, there is no such obvious trend in the relevant behavior of the x component of the correlation function C_{hh}^{xx}, which exhibits the strongest antiferromagnetic short-range correlation shortly after the system passes at the relevant phase boundary to phase II with a fourfold symmetry breaking [see the dotted line for $J_2/J = 0.9$ in Fig. 7(b)].

Furthermore, thermally driven variations of the z and x components of the correlation function between the nearest-neighbor Heisenberg spins are displayed in Figs. 7(c) and 7(d) at the fixed value of the interaction ratio $J_1/J = 4$. These curves bring insight into the effect of temperature upon short-range correlations within the ground states I and III, whereas short-dashed (green) curves correspond exactly to their ground-state phase boundaries given by the constraint $J_2/J = \frac{2J_1/J}{2J_1/J - 1}$. It can be seen that the longitudinal correlation C_{hh}^{zz} is totally absent precisely at the respective phase boundary due to the opposite character of short-range correlation between the nearest-neighbor Heisenberg spins, which is ferromagnetic in character within the classical phase I but antiferromagnetic in the quantum phase III [see Fig. 7(c)]. Moreover, it is quite curious that, above the classical ground state I, the rising temperature contraintuitively causes an uprise of antiferromagnetic correlations in the x component of the correlation function C_{hh}^{xx} in addition to a ferromagnetic-to-antiferromagnetic crossover observable in the z component
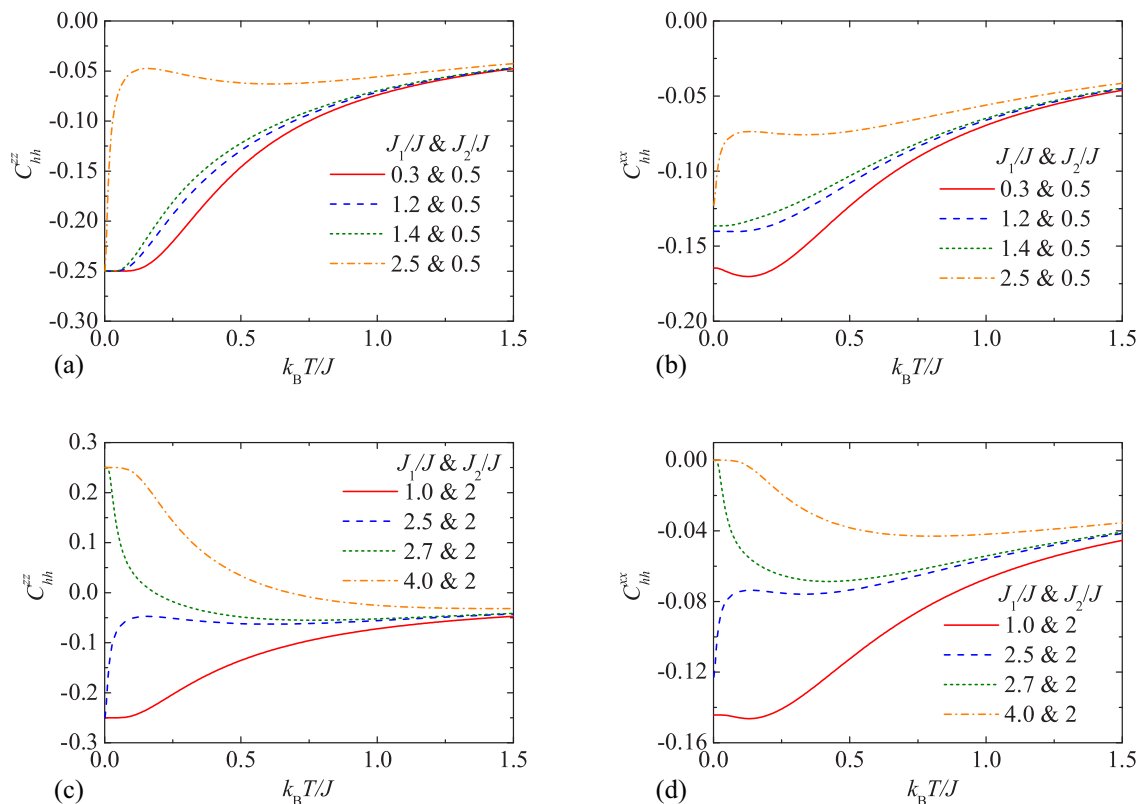
FIG. 6. The correlation function between the z and x components of the nearest-neighbor Heisenberg spins as a function of temperature for a few selected values of the interaction ratio J_1/J and two different constant values of the interaction ratio $J_2/J = 0.5$ (upper panel) and 2 (lower panel).

of the correlation function C_{hh}^{zz} at a certain frustration temperature [40] [see the curves for $J_2/J = 1.2$ in Figs. 7(c) and 7(d)].

The aforementioned results for the correlation function between the nearest-neighbor Heisenberg spins might indicate a highly nontrivial effect of the rising temperature upon their pairwise quantum entanglement, which could in principle be present also above the classical ground state I due to thermal activation of low-lying excited states of a quantum character. In this regard, let us proceed to a discussion of the concurrence depicted in Fig. 8 in the J_1/J-$k_B T/J$ and J_2/J-$k_B T/J$ planes for a few selected values of the coupling constants. The temperature, above which the concurrence becomes zero, can be regarded as a threshold (sudden-death) temperature for the bipartite entanglement (see the solid lines in Fig. 8). Hence, it follows that the nearest-neighbor Heisenberg spin pairs are quantum-mechanically entangled below the displayed line of threshold temperatures, while they become disentangled above it. It can be seen from Fig. 8(a) that the bipartite entanglement is present at sufficiently low temperatures independently of the relative strength of the first Ising interaction J_1/J when the relative strength of the second Ising interaction is fixed to $J_2/J = 0.5$ even though the threshold temperature generally decreases upon strengthening of the interaction ratio $|J_1|/J$. This fact provides independent confirmation of the quantum character of the three ground states III′, II, and III emergent in this parameter space. Contrary to this, the threshold temperature shows a rapid decrease upon increasing the interaction ratio J_1/J until it completely disappears due

to the emergence of the classical ground state I when the relative strength of the second Ising interaction ratio is fixed to $J_2/J = 2$ [see Fig. 8(b)]. It is worthwhile to remark, moreover, that the threshold temperature shows just a relatively small decline when increasing the relative strength of the first Ising interaction in the ferromagnetic counterpart $J_1/J < 0$ of the parameter space.

To get a deeper insight into the effect of the second Ising interaction J_2/J upon the thermal entanglement, the density plot of the concurrence is displayed in Figs. 8(c) and 8(d) in the J_2/J-$k_B T/J$ plane when the relative strength of the first Ising interaction is kept constant, $J_1/J = 2$ or 4, respectively. In the former case, $J_1/J = 2$, one detects nonzero values of the concurrence at sufficiently low temperatures regardless of the coupling ratio J_2/J in accordance with the quantum character of phases II and III being the only two stable ground states in this parameter space. In addition, a gradual decrease of the threshold temperature upon increasing the interaction ratio J_2/J can be attributed to a thermal activation of the classical phase I [see Fig. 8(c)], which becomes close enough in energy to phase II for this set of interaction parameters [cf. Fig. 3(e)]. On the other hand, there are obvious qualitative distinctions in the relevant behavior of the concurrence in the latter case with $J_1/J = 4$ displayed in Fig. 8(d). Under this condition, the threshold temperature decreases monotonically upon increasing the interaction parameter J_2/J until it completely diminishes at the ground-state boundary between phases III and I given by $J_2/J = 8/7$ when assuming $J_1/J = 4$. To summarize, the quantity concurrence implies a slightly stronger
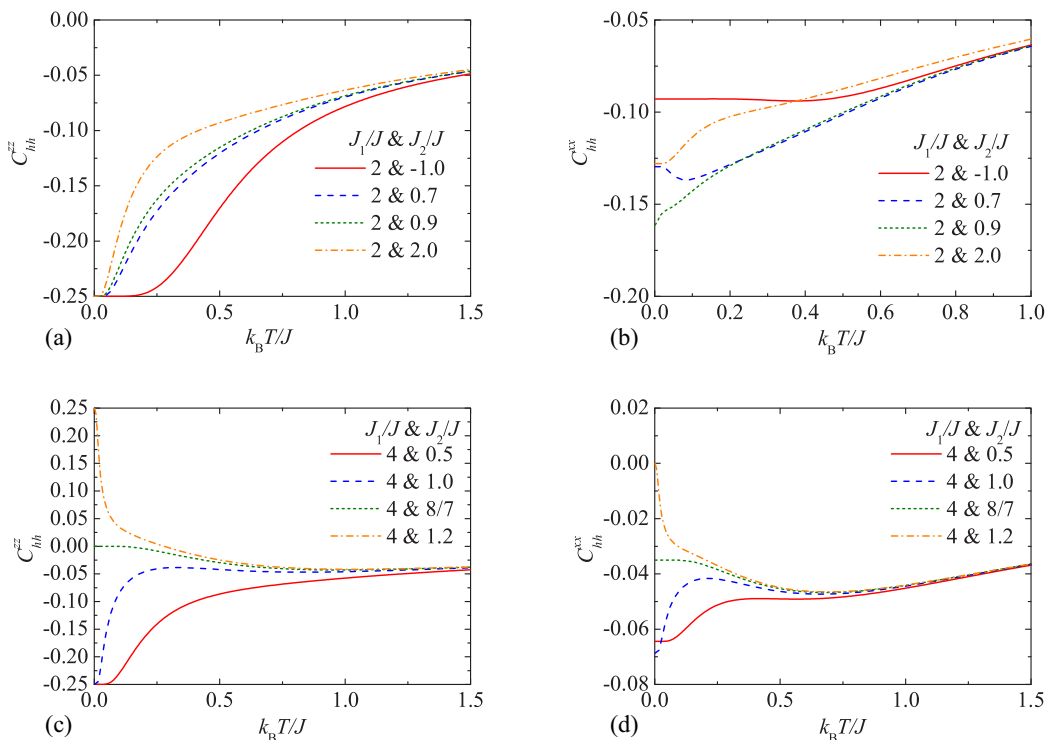
FIG. 7. The correlation function between the z and x components of the nearest-neighbor Heisenberg spins as a function of temperature for a few selected values of the interaction ratio J_2/J and two different constant values of the interaction ratio $J_1/J = 2$ (upper panel) and 4 (lower panel).

quantum entanglement in phase II with a fourfold symmetry breaking compared to phase III without broken symmetry, while the quantum entanglement cannot be thermally induced

above the classical ground state I, although the off-diagonal correlations might be nonzero, as exemplified by the specific case $J_2/J = 1.2$ in Fig. 7(d).
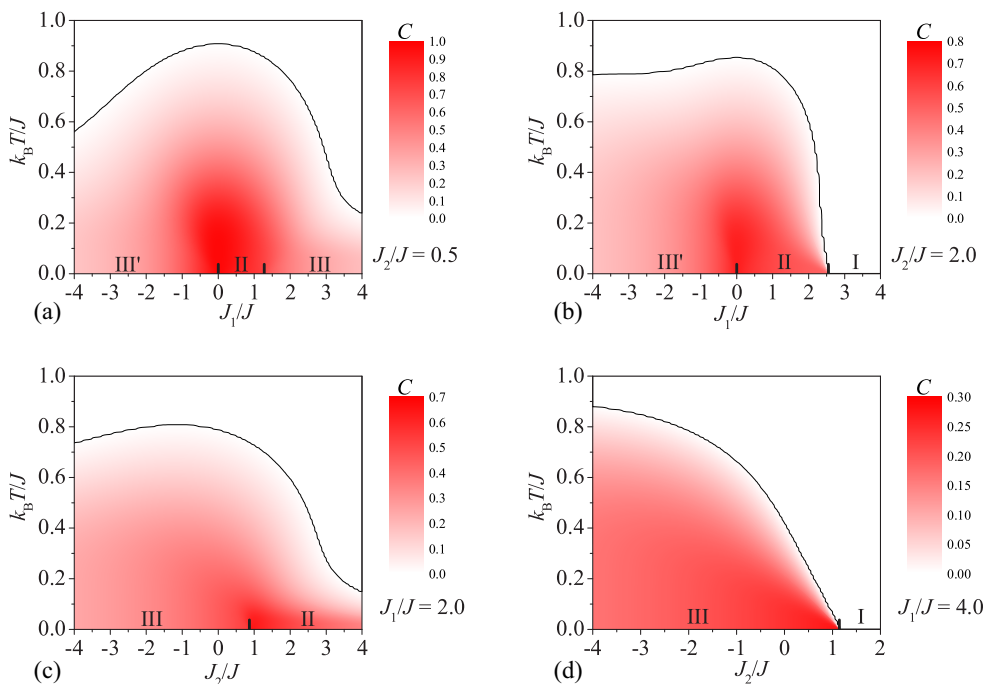

FIG. 8. The density plot of the concurrence in the J_1/J-$k_B T/J$ plane (upper panel) for two selected values of the interaction ratio J_2/J and in the J_2/J-$k_B T/J$ plane (lower panel) for two selected values of the interaction ratio J_1/J. Thick ticks displayed at the x axis correspond to the phase boundaries between the individual ground states.
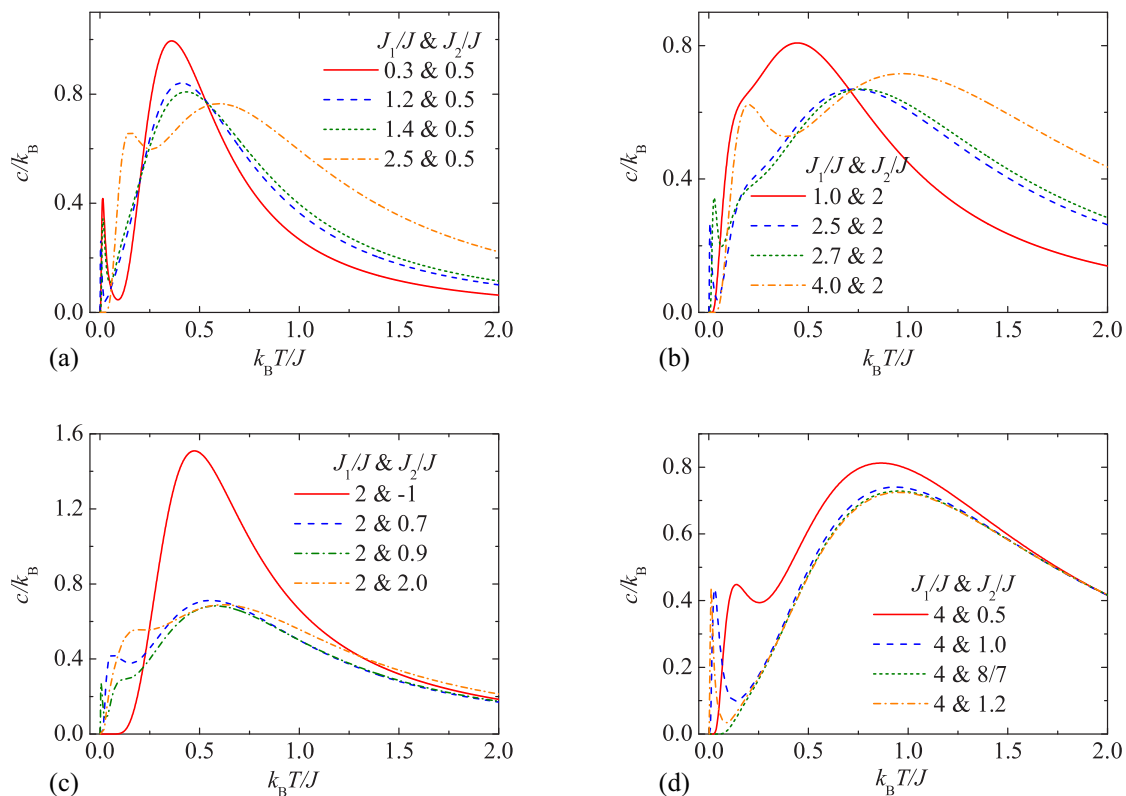
FIG. 9. The specific heat as a function of temperature at several selected interaction ratios J_1/J and J_2/J.

Last but not least, let us discuss typical features of temperature variations of the specific heat, which is depicted in Fig. 9 for the same set of interaction parameters J_1/J and J_2/J as previously used for the discussion of typical thermal dependencies of the pair correlation functions and concurrence. As one can see, the specific heat exhibits either the famous temperature dependence of one-dimensional spin systems with a single round maximum or a more outstanding temperature dependence with two separate maxima. It can be found from Fig. 9 that the marked double-peak structure of the specific heat emerges whenever the interaction parameters drive the spin-$\frac{1}{2}$ Ising-Heisenberg pentagonal chain sufficiently close to one of its ground-state phase boundaries. A relatively sharp low-temperature peak can therefore be attributed to massive thermal excitations from the ground state to a low-lying excited state, which has the character of the phase separated from the ground state by the relevant phase boundary. As a matter of fact, the more the low-temperature peak moves toward lower temperatures and becomes sharper, the closer are the interaction parameters selected to the relevant ground-state phase boundary. On the contrary, the low-temperature peak becomes broader and shifts toward higher temperatures when the interaction parameters are selected farther apart from the relevant ground-state phase boundary until it completely merges with the high-temperature peak. The lack of a low-temperature peak for the particular set of interaction parameters driving the investigated spin system exactly at the ground-state phase boundary also convincingly evidences the aforementioned character of low-lying thermal excitations,

since two ground states have equal energy at their phase boundary, and any other low-lying excited state is missing in the energy spectrum [see the dotted (green) curve for $J_1/J = 4$ and $J_2/J = 8/7$ in Fig. 9(d)].

IV. CONCLUSION

The present article provides exact results for the ground-state phase diagram, pair correlation functions, concurrence, and specific heat of the spin-$\frac{1}{2}$ Ising-Heisenberg pentagonal chain, which are rigorously solved with use of the star-triangle mapping transformation and the transfer-matrix method. All zero-temperature ground states of the spin-$\frac{1}{2}$ Ising-Heisenberg pentagonal chain have been found and completely characterized through the appropriate eigenvectors, which indicate a remarkable diversity of magnetic ground states with the character of a classical ferrimagnetic phase, a classical ferromagnetic phase, two modulated quantum antiferromagnetic phases, a quantum ferromagnetic phase, and a quantum ferrimagnetic phase. The quantum ground states were distinguished from the classical ground states through the concurrence, which has allowed us to quantify the bipartite quantum entanglement between the nearest-neighbor Heisenberg spin pairs.

It should be pointed out that the most spectacular spin arrangement has been found in two modulated quantum antiferromagnetic phases, which exhibit an unusually long period spanned over four unit cells due to a fourfold symmetry breaking that is in sharp contrast with magnetic tetrastability

reported for classical canted spin chains [41]. The existence of fourfold symmetry breaking within the modulated quantum antiferromagnetic phases has been explained in terms of a competition between the effective next-nearest-neighbor and nearest-neighbor interactions of the corresponding spin-$\frac{1}{2}$ Ising zigzag ladder, also known in the literature as the one-dimensional axial next-nearest-neighbor Ising (ANNNI) model [7]. It is also worth noting that the remarkable up-up-down-down ground state of the effective spin-$\frac{1}{2}$ Ising zigzag ladder (ANNNI model) was recently verified using magnetic force microscopy in an artificial spin chain composed of elongated nanomagnets with a controllable ratio between the next-nearest-neighbor and nearest-neighbor interactions [42]. On the other hand, the long-period quantum ground state with a fourfold broken symmetry scarcely appears in one-dimensional quantum spin systems, and it was reported only very recently for the spin-$\frac{1}{2}$ Heisenberg kagomé strip [43]. From this point of view, it is worthwhile to remark that the calculation procedure elaborated on in the present work can be further generalized to a more complex mixed spin-1/2 and

spin-7/2 Ising-Heisenberg pentagonal chain, which is eligible for a theoretical modeling of the heterotrimetallic coordination polymer CuGdFe [26]. This represents a challenging task for future studies.

[1] M. L. Baker, G. A. Timco, S. Piligkos *et al.*, Proc. Natl. Acad. Sci. (USA) **109**, 19113 (2012).

[2] J. Schnack, Dalton Trans. **39**, 4677 (2010).

[3] G. Kamieniarz, W. Florek, and M. Antkowiak, Phys. Rev. B **92**, 140411(R) (2015).

[4] G. Toulouse, Commun. Phys. **2**, 115 (1997).

[5] J. Schnack, C. R. Chim. **10**, 15 (2007).

[6] J. Greedan, J. Mater. Chem. **11**, 37 (2001).

[7] R. Liebman, *Statistical Mechanics of Periodic Frustrated Ising Systems* (Springer-Verlag, Berlin, 1986).

[8] H. T. Diep, *Frustrated Spin Systems* (World Scientific, Singapore, 2013).

[9] C. Lacroix, P. Mendels, and F. Mila, *Introduction to Frustrated Magnetism* (Springer-Verlag, Berlin, 2011).

[10] S. Nellutla, J. van Tol, N. S. Dalal *et al.*, Inorg. Chem. **44**, 9795 (2005).

[11] M. Exler and J. Schnack, Phys. Rev. B **67**, 094440 (2003).

[12] C. Schroder, H. Nojiri, J. Schnack, P. Hage, M. Luban, and P. Kogerler, Phys. Rev. Lett. **94**, 017205 (2005).

[13] M. H. Waldor, W. F. Wolff, and J. Zittartz, Phys. Lett. A **106**, 261 (1984); Z. Phys. B **59**, 43 (1985).

[14] M. Rojas, O. Rojas, and S. M. de Souza, Phys. Rev. E **86**, 051116 (2012).

[15] Z. Gulácsi, Int. J. Mod. Phys. B **27**, 1330009 (2013).

[16] M. Gulácsi, G. Kovács, and Z. Gulácsi, Philos. Mag. Lett. **94**, 269 (2014).

[17] G. Kovács and Z. Gulácsi, Philos. Mag. Lett. **95**, 3674 (2015).

[18] E. Ressouche, V. Simonet, B. Canals, M. Gospodinov, and V. Skumryev, Phys. Rev. Lett. **103**, 267204 (2009).

[19] I. Rousochatzakis, A. M. Läuchli, and R. Moessner, Phys. Rev. B **85**, 104415 (2012).

[20] A. A. Tsirlin, I. Rousochatzakis, D. Filimonov, D. Batuk, M. Frontzek, and A. M. Abakumov, Phys. Rev. B **96**, 094420 (2017).

[21] M. Isoda, H. Nakano, and T. Sakai, J. Phys. Soc. Jpn. **83**, 084710 (2014).

[22] H. Nakano, M. Isoda, and T. Sakai, J. Phys. Soc. Jpn. **83**, 053702 (2014).

[23] A. K. Singh, S. D. Kaushik, B. Kumar *et al.*, Appl. Phys. Lett. **92**, 132910 (2008).

[24] A. M. Abakumov, D. Batuk, A. A. Tsirlin *et al.*, Phys. Rev. B **87**, 024423 (2013).

[25] F. C. Rodrigues, S. M. de Souza, and O. Rojas, Ann. Phys. (NY) **379**, 1 (2017).

[26] R. Gheorghe, M. Andruh, J.-P. Costes, and B. Donnadieu, Chem. Commun. **2003**, 2778 (2003).

[27] M. E. Fisher, Phys. Rev. **113**, 969 (1959).

[28] O. Rojas, J. S. Valverde, and S. M. De Souza, Physica A **388**, 1419 (2009).

[29] J. Strečka, Phys. Lett. A **374**, 3718 (2010).

[30] J. Strečka, *On the Theory of Generalized Algebraic Transformations* (LAP LAMBERT Academic, Saarbrücken, 2010).

[31] H. A. Kramers and G. H. Wannier, Phys. Rev. **60**, 252 (1941).

[32] J. Stephenson, Can. J. Phys. **48**, 1724 (1970).

[33] E. Jurčišinová and M. Jurčišin, Phys. Rev. E **90**, 032108 (2014).

[34] J. M. Yeomans, *Statistical Mechanics of Phase Transitions* (Oxford University Press, Oxford, 1992).

[35] N. Bhattacharyya and S. Dasgupta, J. Phys. A **24**, 3927 (1991).

[36] F. A. Kassan-Ogly, Phase Trans. **74**, 353 (2001).

[37] W. K. Wootters, Phys. Rev. Lett. **80**, 2245 (1998).

[38] L. Amico, R. Fazio, A. Osterloh, and V. Vedral, Rev. Mod. Phys. **80**, 517 (2008).

[39] R. Horodecki, P. Horodecki, M. Horodecki, and K. Horodecki, Rev. Mod. Phys. **81**, 865 (2009).

[40] R. J. V. dos Santos, and M. L. Lyra, Physica A **182**, 133 (1992).

[41] V. Pianet, M. Urdampilleta, T. Colin, R. Clérac, and C. Coulon, Phys. Rev. B **94**, 054431 (2016).

[42] V.-D. Nguyen, Y. Perrin, S. Le Denmat, B. Canals, and N. Rougemaille, Phys. Rev. B **96**, 014402 (2017).

[43] K. Morita, T. Sugimoto, S. Sota, and T. Tohyama, Phys. Rev. B **97**, 014412 (2018).